Article:

Lamy-Chappuis, B, Angus, DAC orcid.org/0000-0003-0734-7835, Fisher, Q et al. (1 more author) (2016) The effect of CO2-enriched brine injection on the mechanical properties of calcite bearing sandstone. International Journal of Greenhouse Gas Control, 52. pp. 84-95. ISSN 1750-5836

https://doi.org/10.1016/j.ijggc.2016.06.018

The effect of CO_2-enriched brine injection on the mechanical properties of calcite-bearing sandstone.

Authors

Benoit Lamy-Chappuis, Doug Angus, Quentin J. Fisher and Bruce W.D. Yardley, School of Earth and Environment, University of Leeds

Corresponding author

Benoit Lamy-Chappuis, School of Earth and Environment, University of Leeds, LS2 9JT, United Kingdom. Email: benoit.lamychappuis@gmail.com.

Abstract

The mechanical and fluid-flow response of subsurface geological reservoirs due to injection of CO_2 is of critical importance for the safe management and storage of anthropogenic carbon emissions. Although the time-lapse seismic method has proven to be an effective tool to remotely monitor changes in underground fluid saturations, variations in reservoir properties caused by geochemical interactions can also influence the seismic response. This can lead to ambiguity and uncertainty in monitoring the movement of injected CO_2 and hence determination of reservoir seal integrity. Geochemical interactions can also modify the mechanical strength of the reservoir and therefore threaten its integrity. We conducted experiments to assess how the velocity and rock strength of a calcite-bearing sandstone are affected by flooding with CO_2 saturated brine. The results indicate that both seismic velocity and rock strength are significantly reduced due to minor calcite dissolution. The implications at the reservoir scale for CO_2 storage are twofold. Firstly, modifications in velocity can complicate seismic monitoring operations and lead to interpretation errors. This can be

accounted for if shear wave velocity variations are used to detect fluid-rock interactions. Secondly, reduction in rock strength, caused by calcite dissolution, can threaten reservoir and wellbore integrity under stress conditions typically found in potential carbon repositories.

Keywords.

Carbon storage, Fluid-rock interactions, Yield stress, Sonic velocity

1. Introduction

Monitoring CO_2 injection is an essential component of the geological carbon storage (GCS) chain as it can condition public acceptance and will likely be necessary to comply with regulations. Time-lapse seismic methods have generally been considered to be a sufficiently accurate means of monitoring CO_2 saturation in the subsurface in terms of both the flow and the storage of injected CO_2 for various GCS pilot studies (Cook, 2014; White, 2013; Chadwick et al., 2010; Daley et al., 2008). To increase the confidence in this method it is essential to understand how geochemical interactions triggered by CO_2 injection modify the mechanical response of the reservoir and surrounding rocks (Vanorio et al., 2011; Hangx et al., 2013; Clark and Vanorio, 2016). Rock sonic velocity has a directly influence on seismic imaging while rock deformation can also lead to noticeable effects in time-lapse seismic analysis (e.g., Herwanger and Koutsabeloulis, 2011). Rock mechanical properties also influence the injection operations by constraining the maximum safe injection pressure and controlling fault reactivation, reservoir deformation and in turn wellbore and caprock integrity. Consequently, we focus on two properties of interest which are the rock seismic velocity and the rock strength.

In saline aquifers repositories, CO_2 dissolution in brine can lead to brine acidification, one direct consequence is the dissolution of carbonate minerals and hence a modification of the rock framework and mechanical behaviour. Vanorio et al. (2011) studied salt precipitation and carbonate dissolution effects in limestone and concluded that they were significant for modelling and interpreting time-lapse seismic signals. The hypothesis that geochemical effects could be significant is appealing since it could explain some inconstancies between measured and predicted velocities that have been observed at various GCS sites. For example, a larger than expected velocity slowdown was observed at Frio (Daley et al., 2008). In particular, the S wave velocity decrease could indicate a change in the rock frame as this parameter is supposedly insensitive to changes in pore fluids. Hangx et al. (2013) found that sonic velocity and rock strength were not significantly affected by small amounts of carbonate dissolution because the rock was quite quartz cemented. They concluded that "for less quartz-cemented sandstones there may be an increased risk for calcite-dissolution-induced weakening".

In this paper, experimental results obtained from rock cores of a sandstone collected from Cayton Bay, NE England, are used to illustrate the effects of calcite dissolution triggered by reaction with CO_2 on sonic velocity and mechanical properties. Minor amount of calcite dissolution has already been shown to significantly enhance the permeability of the Cayton Bay sandstone (Lamy-Chappuis et al., 2014). In the current study, a flow through reactor apparatus was used to dissolve calcite from cores that were then subjected to series of sonic velocity and strength measurements. The comparison with baseline values revealed a significant reduction in sonic velocity and strength. The consequences for GCS management need to be discussed.

2. Sonic velocity

2.1 Sonic velocity usage and limitations for GCS

Sonic velocity data is routinely used to quantify fluid saturation, porosity and the lithology of underground reservoirs (Sheriff and Geldart, 1995). Time-lapse seismic monitoring is the most relevant technique to track changes in fluid distributions during reservoir production (Calvert, 2005), it is based on the interpretation of changes in seismic properties (e.g., reflection, travel-times and amplitudes). This technology is viewed as an essential tool to monitor fluid injection and fluid flow for GCS projects (Chapman et al., 2000; Arts et al., 2004; Brown et al., 2002; Li, 2003). It is also thought that detailed interpretation of time-lapse seismic data could provide pore pressure information (Grude et al., 2013, White et al., 2015).

Traditionally, changes in seismic response may primarily be attributed to saturation changes due to fluid substitution stemming from CO_2 injection. The effect of fluid substitution can be modelled using the Gassmann and Biot equations (Gassmann, 1951; Biot, 1956a, b; Mavko and Jizba, 1991; Han and Batzle, 2004). By default, these equations do not address the effects of geochemical interactions on the rock frame behaviour, which could lead to interpretation errors. This is important because it has been recognized that the elastic behaviour of rock is nonlinearly dependent on stress (Walsh, 1965a, 1965b; Nur and Simmons, 1969) and so any modifications of the mechanical strength of the rock can influence the stress dependent behaviour (Verdon et al. 2008). In addition, geochemical interactions could lead to changes in mechanical strength and to deformation manifested in time-lapse seismic effects (e.g., Herwanger and Koutsabeloulis, 2011). It is therefore useful to compare the impacts of fluid substitution and calcite dissolution on sonic velocity.

2.2 Experimental design

The experimental setup consisted of a triaxal cell instrumented for ultrasonic velocity measurement under variable pressure and fluid saturation conditions (Figure 1). The vertical press was programmed to perform an axial loading and unloading cycle while the lateral pressure was manually controlled with an external pump to maintain isostatic conditions. Experiments were done at a temperature of 50±2°C (above the critical temperature of CO_2).

Piezoelectric transducers mounted at the ends of steel platens were used to generate a 1 MHz P wave and two 0.7 MHz orthogonally polarized S waves to measure a fast and slow shear wave. A disk of lead foil was placed in either end of the sample to improve the contact between the transducers and the cores. Travel times were determined for the first peaks corresponding to the sonic wave's arrivals and were zeroed by doing a measurement with no rock core. The difference in orthogonal S waves velocities at any fluid saturation conditions never exceeded 0.3%, meaning that the rock cores were fairly isotropic. For simplicity, in the remainder of this paper the average S wave velocity is reported.

Rock cores were drilled with a diameter of 3.75 cm, carefully cut to a length of 7.30-7.80 cm, with special care to ensure that the ends were perfectly perpendicular to the axis of the core plugs. The cores were then dried in an oven for 48 h at 60°C. The samples were then left dry or saturated with CO_2 or brine under vacuum, the saturating fluids would then be pressurized with an external ISCO pump and heated in a core holder. All experiments were done in drained conditions (i.e. fluids were allowed to move in and out of the sample).

Pressure conditions were chosen to span a large range of relevant in-situ reservoir conditions. The pore pressure was varied between 3.4 and 27.5 MPa. Lateral confining pressure and axial load were varied between 6.9 and 69 MPa and were kept isostatic. The resulting effective pressure for each experiment ranged between 3.5 and 41.5MPa (effective pressure = confining pressure - pore pressure). Various experimental conditions were used to examine the effect of fluids, fluid pressure and calcite dissolution on the sonic velocity, see Table 1.

2.3 Results

2.3.1 Rock and fluid controls on velocity

A preliminary series of measurements was done on unaltered samples to evaluate the effect of effective stress, pore pressure and fluid composition (either 1M NaCl brine or CO_2) on sonic velocity, this experiment serves as a base case where geochemical interactions are neglected.

Figure 2 presents sonic velocity data obtained on one core (core number 3.1) at varying effective stress conditions imposed by a confining pressure loading and unloading cycle (the pore pressure is kept constant during each cycle). There is a clear influence of the effective pressure on the sonic velocity that shows a consistent increase with effective stress at all fluid saturation conditions. The velocities tend to converge at the maximum confining/effective pressures, this is generally attributed to micro-cracks and compliant pores closing within increasing stress and to interactions at the grain boundaries. This effect is reversible since the velocity curves are almost the identical during the loading and unloading paths. The low amount of hysteresis is a good indication that the samples were not damaged during loading and thus could be re-used for further experiments.

S wave velocity (Vs) decreases gradually with increasing CO_2 pressure (i.e. with increasing CO_2 density). Brine saturated samples have the lowest velocities, which is consistent with brine having the highest density at all studied pressures. Brine being incompressible, the sonic velocity in the brine-saturated case does not depend on fluid pressure (for a given effective pressure). The pattern is different for the Vp where the slowdown does not exactly follow the density trend. This difference is due to brine having a bulk modulus that is several orders of magnitude larger than that of CO_2 and this partly counterbalances the effect of density on the velocity. As a result, the V_P/V_S ratio is significantly higher when the rock is brine saturated and this is known to be a very good indicator of the type of fluid substitution. Overall it is clear that the changes in fluid density dominate the differences in velocities for this experiment. In particular, the observed velocities under fluid saturated conditions are lower than in the dry case and are consistent with Gassmann equation calculations (see Appendix B) where we only took into account density variations and neglected high frequency viscous effects (i.e. squirt flow). There is however a general overestimation of the velocities calculated with Gassmann equations, especially (but not limited to) the brine-saturated cores. This fall within the uncertainty of the Gassmann equation input parameters but could also point towards a secondary effect affecting the experimental results. One possibility is that the dry cores were “over-dried” leading to an overestimation of the dry cores bulk modulus which is used in Gassmann equation to calculate the sonic velocity of the fluid-saturated rock. The other possibility is that the fluids have a “lubrication” effect whereby the rock frame is weakened and produce anomalously low S and P waves velocities. This is consistent with the brine-saturated measurements being particularly affected since brine has a much higher wettability than CO_2 at our experimental conditions.

2.3.2 Impact of calcite dissolution on sonic velocity

Four experiments have been conducted on dry cores (cores 2.1, 3.1, 3.2 and 4.1) to evaluate the change in sonic velocity after calcite dissolution. We used only dry cores in order to suppress the possibility of ambiguous interpretation caused by the introduction of fluids and because this is relevant to common industry practice whereby the properties of fluid-saturated rocks are predicted from their dry counterpart using Gassmann equations. As previously described in Lamy-Chappuis et al. (2014), the Cayton Bay sandstone contains dispersed shell fragments accounting for about 5% of the grain volume (Figure 3) and their dissolution has already been shown to have a rapid and significant effect on transport properties. No other significant geochemical reactions were recorded. In particular, clays, which are known to affect sonic velocity, were unaffected by CO_2-saturated brine flooding (Lamy-Chappuis et al., 2014). For each core, the porosity was recorded before and after total calcite dissolution using helium porosimetry. Sonic velocity measurements done before and after calcite removal are shown in Figure 4.

The main features of Figure 4 are the large variability in initial sonic velocities and the significant velocity slowdown after calcite dissolution for all cores. A striking observation is that the decrease in velocity is comparable to the one caused by fluid substitution (as shown in Figure 2), roughly 10 ± 5% decrease depending on the porosity change. This slowdown applied to V_P and V_S in a similar fashion so that the V_P/V_S ratio was left relatively unchanged.

Eq. (1) was used to calculate the bulk and shear moduli from sonic velocity data, before and after calcite dissolution.

$$K_{dry} = \rho\left({V_P}^2 - \frac{4}{3}V_S^2\right) \text{ and } M_{dry} = \rho V_S^2, \qquad (1)$$

where K_{dry} is the dry rock bulk modulus, M_{dry} is the dry rock shear modulus and ρ is the rock density.

Figure 5 reveals that both parameters were reduced to an average of 80% of their initial value and the dissolution effect is quite insensitive to the effective pressure conditions. This means that the pores created by calcite dissolution were not significantly more or less compliant than the original pores. Also, calcite dissolution did not modify the stress sensitivity of the poroelastic response as could be the case if calcite was found as a cement (rather than as isolated fragments) or at grain boundaries.

The velocity is in fact closely correlated to the absolute porosity value. The natural porosity variation and the one caused by calcite dissolution produces the same trends when plotting velocities against porosity (Figure 6). This supports the idea that for a given rock texture the absolute porosity is the primary variable upon which sonic velocity depends. This is the idea behind classical velocity-porosity correlations such as the Wyllie time average equation or more advanced empirical correlations (Raymer et al., 1980; Han et al., 1986; Tosaya and Nur, 1982; Castagna et al., 1985).

The experimental correlation from Han is very accurate in term of absolute velocity prediction based solely on porosity and clay content although the velocity gradient with porosity is lower than in the present experiments. Other correlations obtained on water-saturated samples (e.g, Tosaya and Castagna correlations) unsurprisingly do not predict the absolute “dry” velocities but are better at predicting the relative slowdown caused by calcite dissolution (Figure 7). All the equations for these correlations can be found in Mavko et al. (2009) and in Appendix A.

2.3.3 Significance for time-lapse seismic monitoring of GCS

By using the experimental data it is possible to construct a CO_2 injection scenario and identify the best indicators for tracking fluid substitution and calcite dissolution. Figure 8 shows a possible time sequence (from left to right). The initial reservoir state (left column) is 100% brine saturation with a pore pressure of 14 MPa and an effective pressure of 14 MPa. The second stage (second column from left) retains the same fluid saturation but the brine pore pressure has been increased to 21 MPa and hence a reduction in effective pressure to 7 MPa. In the third stage (third column from left) the brine has been fully replaced by CO_2 at the same pore pressure of 21 MPa. The last stage (column on the right) is an end-member case including both fluid substitution and calcite dissolution effects (i.e., reduction of mechanical strength) on the velocities. Note that in the figure, all velocities are normalized to an initial velocity, which value as been arbitrarily set to 100.

For the P wave velocity, the change in fluid pressure has a small effect. However, fluid substitution reduces the velocity by roughly 10% and calcite dissolution reduces the velocity by another 10%. For the same sequence of stages, the only significant change in S wave velocity is due to calcite dissolution (about 10% decrease). The ratio V_P/V_S is essentially constant during reservoir pressurization and calcite dissolution, yet is strongly sensitive to fluid substitution. The results of this analysis suggests that V_P/V_S should be used to detect replacement of formation water by CO_2 and V_S alone should be used to detect changes in the rock frame due to mineral dissolution.

Only considering V_P during time-lapse seismic analysis could lead to large interpretation errors. Figure 9 shows the evolution of the P wave velocity with fluid substitution calculated with Gassmann equations (see Appendix B). The bulk modulus of the brine-CO_2 mixture was calculated with Wood's equation (Wood, 1941). For the "Normal fluid substitution" curve only the CO_2 saturation was varied. For the "Fluid substitution and increase in porosity" curve the fluid rock interactions were incorrectly taken into account by simply increasing the porosity parameter in Gassmann equation. The last curve is the most accurate as it takes into account fluid-rock interaction effects on both porosity and K_{dry} parameters (as evaluated in the present experiments, details can be found in Appendix B).

It appears that a few percent of CO_2 saturation associated with calcite dissolution (lower curve) could be misinterpreted as 100% CO_2 infiltration with no proper account of calcite dissolution (upper curves). In practice the true V_P-saturation curve will lie between the two end-member curves as calcite dissolution and CO_2 invasion happen simultaneously.

This indicates that a detailed analysis of the sonic velocity changes is recommended to discriminate between the effects of fluid substitution and rock frame modification. Detailed velocity analysis may not necessary if the purpose of time-lapse monitoring is simply intended to detect CO_2 leaks into the overlying geological layers. However, detailed analysis is recommended if the purpose of time-lapse monitoring is to track accurately the CO_2 propagation or quantify localized fluid-rock interactions in the reservoir and in the surrounding layers. Localization and quantification of rock frame modifications could be useful to monitor and prevent reservoir and wellbore deformation (Kristiansen and Plischke, 2010). In this framework, the following section addresses the consequences of calcite dissolution for the strength of the Cayton Bay sandstone. It is important to know if, for a given reservoir stress state, geochemical reactions can significantly weaken the rock and consequently lead to rock yielding or failure. Yielding or failure could compromise both wellbore and formation stability as well as reduce the reservoir permeability.

3 Peak and yield strength

3.1 Experimental design

Multiple failure experiments were used to obtain peak and yield stress data points at increasing confining pressures. The experiment proceeds as series of single failure tests where the confining pressure is quickly increased to reestablish isostatic pressure when the sample starts to fail. Usually strength results obtained from multistage tests are systematically lower than results from single-stage tests because the sample gets weaker as it becomes slightly damaged by incipient yielding and fracturing at each stage. This technique is, however, less time consuming and works very well on relatively plastic rocks where failure does not occur dramatically and confining pressure can be increased on time. It also removes issues regarding sample heterogeneity compared to when the failure envelop is measured based on multiple single-failure experiments.

Initial tests on Cayton Bay sandstone indicated that the multiple failure test was well suited to this rock, which is quite plastic under the stress conditions used. Two separate sets of cores were used, one unreacted and the other one where the calcite had been dissolved. Nine multiple failure test were conducted on water saturated cores in drained conditions and at room temperature.

A triaxial testing machine was equipped with LVDT (Linear Variable Displacement Transducer) to record the axial strain. The LVDT result from one experiment is shown in Figure 10. After each confining pressure increase, axial unloading and reloading cycle was performed, allowing the rock to return into the elastic domain.

The yield points are defined as the points where the curve departs from the linear elastic trend. The confining pressure was increased in seven stages at 5, 10, 20, 30, 40, 50 and 60 MPa. After the last stage was reached the confining pressure was gradually reduced to evaluate the residual strength of the rock. In general, the onset of rock failure occurred at 10MPa above the yield point.

3.2 Calcite dissolution effect on rock strength

The yield stress envelope created by plotting all yield points on a σ_1-σ_3 plot (Figure 11) shows that calcite dissolution effectively decreased the strength of the rock.

For illustration the σ_1-σ_3 state for a hypothetical reservoir where faults with a friction coefficient of 0.85 constrain the stress state is shown in Figure 11. The calculation used a continuous underground rock density of 2800 kg.m^{-3}, which represents a hypothetical average density of rocks situated above a layer of Cayton bay sandstone, and assumed that the pore pressure was hydrostatic. Three points are shown, corresponding to the state in the reservoir at depths of 1000, 2000 and 3000m. In the ideal case, (Jaeger and Cook, 1979) the ratio of $\sigma_1 - P_f$ to $\sigma_3 - P_f$ is a function of the fault friction coefficient μ as follows:

$$\frac{\sigma_1 - P_f}{\sigma_3 - P_f} = \left(\sqrt{\mu^2 + 1} + \mu\right)^2 \quad (2)$$

where P_f is the pore pressure. For a normal faulting regime σ_1 is the vertical stress, equal to $\rho g z$, then at 1000 m $\sigma_1 - P_f$ = 18 MPa and $\sigma_3 - P_f$ = 4 MPa. Similarly for 2000 m $\sigma_1 - P_f$ = 36 MPa and $\sigma_3 - P_f$ = 8 MPa; for 3000 m, $\sigma_1 - P_f$ = 54 MPa and $\sigma_3 - P_f$ = 12 MPa.

The curves in Figure 11 indicate that it is possible for calcite dissolution to trigger ductile yielding in the hypothetical reservoir at a depth of about 2000 m, at this depth the yield stress of the reacted samples are all inferior to the reservoir principal stress. At 1000 m none of the samples would yield while at 3000m only two unreacted samples would not yield.

The decrease in rock strength is likely due to a decrease in rock cohesion and in the angle of internal friction. Rewriting the Coulomb law of failure as:

$$\sigma_1 = \frac{2\tau_0 \cos\varphi}{1-\sin\varphi} + \sigma_3 \frac{1+\sin\varphi}{1-\sin\varphi} \qquad (3)$$

where τ_0 is the rock cohesion and φ is the angle of internal friction; linear fits to average peak envelopes before and after calcite dissolution (Figure 12) translates into τ_0 decreasing from 14.5 to 10.5 MPa and φ decreasing from 16.0 to 8.3°.

On Figure 10 there is no clear break between results for reacted and unreacted cores. The yield stress curves are shown as a function of porosity in Figure 13. These results suggest that the decrease in strength is a strong function of porosity, irrespective of whether it is original or secondary. This result is analogous to the one obtained on sonic velocity.

4. Conclusion

The experimental results presented here provide very strong evidence that fluid rock interactions cannot be neglected when dealing with the mechanical properties of calcite bearing reservoirs in the context of GCS. They show large modifications of the sonic velocity and rock strength parameters upon calcite dissolution. For instance, this study shows that a 10% porosity increase can provoke a 10% decrease in sonic velocity which is the same order of magnitude as the velocity decrease expected during fluid substitution from brine to supercritical CO_2.

The results show that a good first order prediction of the velocity change upon calcite dissolution can be achieved by using simple correlations found in the literature. Care should be taken before generalizing this result since this study only examined the effect of a small amount of calcite dissolution in the form of isolated shell fragments. It is also worth noting that these fragments had similar sizes to the pre-existing pores (approximately 100 μm diameter). It is possible that different sandstone textures would produce different results depending on the nature of the reactive minerals, their proportion in the rock and their placement in the rock frame.

At the reservoir scale the possible implications of this study are twofold. Firstly, the work conducted on sonic velocity demonstrates the fluid-rock reactions must be accounted for to properly interpret seismic data in terms of fluid saturation. Secondly the study of the yield and peak envelopes demonstrates that fluid-rock interactions can in some circumstances be a threat to reservoir and/or well integrity by reducing rock strength and triggering irreversible plastic deformation. However, rock compaction after yielding could mitigate this effect by increasing rock strength. The exact implications of this work at the reservoir scale will depend on the extent and localization of calcite dissolution.

The changes in porosity and rock properties associated with fluid-rock reactions could be calculated and localized with time-lapse seismic surveys of P and S wave components. This could provide a means to assess the reservoir and well instability risk and would necessitate an integrated reservoir mechanical modelling that is out of the scope of this study.

The correlation between porosity and rock mechanical properties is very strong in these experiments, such that the effect of natural porosity variations is almost independent of whether porosity is original or created experimentally by calcite dissolution. This conclusion is very different from the one reached for the transport properties in Lamy-Chappuis et al. (2014). In their study of the Cayton Bay sandstone, the changes in transport properties depended on the change in pore network morphology rather than on the absolute change in pore volume, this is the opposite for the sonic velocity and rock strength properties. Nevertheless, it is not possible to generalize this result to all calcite bearing sandstones as it seems logical that in some conditions the pore morphology would have a larger influence.

Acknowledgments

This work was supported by EPSRC research grant reference EP/I010971/1. We are indebted to John Martin for his assistance with the experimental and analytical procedures. We also would like to thank Jens Birkholzer and three anonymous reviewers for their challenging and constructive comments.

I. Appendix A

Details of empirical sonic velocity-porosity correlations used for Figures 6 and 7.

Raymer: $V_P = 5800\,(1-\theta)^2$ m/s

Han: $V_P = 5410 - 6350\,\theta - 2870\,c$ m/s

$V_S = 3570 - 4570\,\theta - 1830\,c$ m/s

Tosaya: $V_P = 5800 - 8600\,\theta - 2400\,c$ m/s

Castagna: $V_P = 5810 - 9420\,\theta - 2210\,c$ m/s

All equations are applicable for the Cayton Bay sandstone which has a porosity θ of 30% and a clay content c of 5%.

II. Appendix B

The Gassmann equation has been used to predict the change in sonic velocity caused by changes in fluid saturation. According to these equations the bulk and shear moduli of a fluid saturated rock can be calculated with the separate mechanical properties of the dry rock and fluid:

$$K_{sat} = K_{dry} + \frac{\left(1-\frac{K_{dry}}{K_m}\right)^2}{\frac{\phi}{K_{fl}}+\frac{1-\phi}{K_m}-\frac{K_{dry}}{K_m^2}}$$

$$M_{sat} = M_{dry}, \qquad \text{(B1)}$$

where K_{sat}, K_{dry}, K_m, and K_{fl} are the bulk moduli of the saturated rock, dry rock, mineral composing the rock and saturating fluid respectively; M_{sat} and M_{dry} are the shear moduli of the saturated and dry rock; ϕ is the rock porosity. This equation allows the estimation of seismic velocities of rocks saturated with various fluids when knowing dry rock velocities.

Figure 9 calculation of the fluid substitution curve accurately including calcite dissolution effects:

For K_{dry} the experimental data obtained on sample 3.1 was employed (this experiment produced an intermediate reduction of K_{dry} by about 20%) , K_m was calculated using the Voight-Reuss-Hill average (Hill, 1952) from the data shown in table B1.

K_{fl} for CO_2 and brine were calculated from speed of sound equations of Span and Wagner (1996) and Batzle and Wang (1992) for CO_2 and brine respectively. For the Gassmann modelling the rock density was taken as 1780 kg/m^3, porosity as 32.5% and K_m as 34.5 MPa (these are averages over all Cayton Bay rock cores); other parameters used for the modelling are shown in table B2. The shear modulus of the fluid-rock system is assumed to be equal to that of the dry rock frame since CO_2 and brine have no shear strength under liquid and supercritical conditions, see Eq. (B1).

References

Arts R., Eiken O., Chadwick A., Zweigel P., van der Meer L. and Zinszner B., Monitoring of CO2 injected at Sleipner using time-lapse seismic data, *Energy* **29** (9–10), 2004, 1383–1392, http://dx.doi.org/10.1016/j.energy.2004.03.072.

Batzle, M. and Wang, Z., Seismic properties of pore fluids. *Geophysics* **57** (11), 1992, 1396–1408. http://dx.doi.org/10.1190/1.1443207.

Biot M.A., Theory of propagation of elastic waves in a fluid-saturated porous fluid. 1. Low frequency range, *J. Acoust. Soc. Am.* **28** (2), 1956a, 168–178, http://dx.doi.org/10.1121/1.1908239.

Biot M.A., Theory of propagation of elastic waves in a fluid-saturated porous fluid. 2. Higher frequency range, *J. Acoust. Soc. Am.* **28** (2), 1956b, 179–191, http://dx.doi.org/10.1121/1.1908241.

Brown L.T., Integration of Rock Physics and Reservoir Simulation for the Interpretation of Time-Lapse Seismic Data at Weyburn Field, Saskatchewan, 2002, Colorado School of Mines.

Calvert R., 4D technology: where are we, and where are we going?, *Geophys. Prospect.* **53** (2), 2005, 161–171, http://dx.doi.org/10.1111/j.1365-2478.2004.00469.x.

Castagna J.P., Batzle M.L. and Eastwood R.L., Relationships between compressional-wave and shear-wave velocities in clastic silicate rocks, *Geophysics* **50** (4), 1985, 571–581, http://dx.doi.org/10.1190/1.1441933.

Chadwick R.A., Williams G.A., Williams J.D.O. and Noy D.J., Measuring pressure performance of a large saline aquifer during industrial-scale CO2 injection: the Utsira Sand, Norwegian North Sea, *Int. J. Greenh. Gas Control* **10**, 2012, 374–388, http://dx.doi.org/10.1016/j.ijggc.2012.06.022.

Chapman M., Zatsepin S. and Crampin S., Time-lapse seismic changes in a CO2 injection process in a fractured reservoir [Exp. Abs.], *Soc. Explor. Geophys.* 2000, 1536–1539.

Clark A.C. and Vanorio T., The rock physics and geochemistry of carbonates exposed to reactive brines, *J. Geophys. Res. Solid Earth* **121**, 2016, 1497–1513, http://dx.doi.org/10.1002/2015JB012445.

Cook, P., Geologically storing carbon: Learning from the Otway Project experience, 2014, CSIRO Publishing. ISBN: 9781486302307.

Daley T.M., Myer L.R., Peterson J.E., Majer E.L. and Hoversten G.M., Time-lapse crosswell seismic and VSP monitoring of injected CO2 in a brine aquifer, *Environ. Geol.* **54** (8), 2008, 1657–1665, http://dx.doi.org/10.1007/s00254-007-0943-z.

Gassmann, F., Uber die Elastizitat poroser Medien, Mitteiluagen aus dem Inst. fur Geophysik (Zurich), 17, 1951, 1-23. Translated and reprinted as: On elasticity of porous media, in Classics of Elastic Wave Theory, *Soc. Explor. Geophys,* 2007, http://dx.doi.org/10.1190/1.9781560801931.ch3p.

Grude S., Landrø M. and Osdal B., Time-lapse pressure-saturation discrimination for CO2 storage at the Snøhvit field. *Int. J. Greenh. Gas Control* 19, 2013, 369–378, http://dx.doi.org/10.1016/j.ijggc.2013.09.014

Han D.H. and Batzle M.L., Gassmann's equation and fluid-saturation effects on seismic velocities, *Geophysics* **69** (2), 2004, 398–405, http://dx.doi.org/10.1190/1.1707059.

Han D., Nur A. and Morgan D., Effects of porosity and clay content on wave velocities in sandstones, *Geophysics* **51** (11), 1986, 2093–2107, http://dx.doi.org/10.1190/1.1442062.

Hangx S., van der Linden A., Marcelis F. and Bauer A., The effect of CO2 on the mechanical properties of the Captain Sandstone: geological storage of CO2 at the Goldeneye field (UK), *Int. J. Greenh. Gas Control* **19**, 2013, 609–619, http://dx.doi.org/10.1016/j.ijggc.2012.12.016.

Herwanger J. and Koutsabeloulis N., Seismic Geomechanics: How to Build and Calibrate Geomechanical Models Using 3D and 4D Seismic Data, 2011, EAGE Publications. ISBN: 978-90-73834-10-1.

Hill R., The elastic behavior of a crystalline aggregate, *Proc. Phys. Soc* **65** (5), 1952, 349-354. http://dx.doi.org/10.1088/0370-1298/65/5/307

Jaeger J. and Cook N., Fundamentals of Rock Mechanics, 1979, Mathuen; London.

Kristiansen, T.G. and Plischke B., History matched full field geomechanics model of the Valhall Field including water weakening and re-pressurisation, *Soc. Explor. Geophys.* 2010, http://dx.doi.org/10.2118/131505-MS

Lamy-Chappuis B., Angus D., Fisher Q., Grattoni C. and Yardley B.W.D., Rapid porosity and permeability changes of calcareous sandstone due to CO2-enriched brine injection, *Geophys. Res. Lett.* **41**, 2014, 399–406, http://dx.doi.org/10.1002/2013GL058534.

Li G., 4D seismic monitoring of CO2 flood in a thin fractured carbonate reservoir, *Lead. Edge* **22** (7), 2003, 690–695, http://dx.doi.org/10.1190/1.1599698.

Mavko G. and Jizba D., Estimating grain-scale fluid effects on velocity dispersion in rocks, *Geophysics* **56** (12), 1991, 1940–1949, http://dx.doi.org/10.1190/1.1443005.

Mavko G., Mukerji Tapan and Dvorkin J., The Rock Physics Handbook, 2009, Cambridge University Press.

Nur A. and Simmons G., The effect of saturation on velocity in low porosity rocks, *Earth Planet. Sci. Lett.* **7**, 1969, 183–193.

Raymer L.L., Hunt E.R. and Gardner J.S., An Improved Sonic Transit Time-To-Porosity Transform, 21st SPWLA Annual Meeting, Society of Petrophysicists and Well Log Analysts, 1980, 1-13.Sheriff R.E. and Geldart L.P., Exploration Seismology, 1995, Cambridge Univ. Press; New York, 592 pp.

Span R. and Wagner W., A New Equation of State for Carbon Dioxide covering the Fluid Region from the Triple-point Temperature to 1100 K at Pressures up to 800 MPa, *J. Phys. Chem. Ref. Data* **25** (6), 1996, 1509–1596, http://dx.doi.org/10.1063/1.555991.

Tosaya C. and Nur A., Effects of diagenesis and clays on compressional velocities in rocks, *Geophys. Res. Lett.* **9** (1), 1982, 5–8, http://dx.doi.org/10.1029/GL009i001p00005.

Vanorio T., Nur A. and Ebert Y., Rock physics analysis and time-lapse rock imaging of geochemical effects due to the injection of CO2 into reservoir rocks, *Geophysics* **76** (5), 2011, O23–O33, http://dx.doi.org/10.1190/geo2010-0390.1.

Verdon J., Angus D.A., Kendall J.-M. and Hall S., The effects of micro- structure and nonlinear stress on anisotropic seismic velocities, *Geophysics* **73** (4), 2008, D41–D51, http://dx.doi.org/10.1190/1.2931680.

Walsh J., The effect of cracks on the compressibility of rock, *J. Geophys. Res.* **70**, 1965a, 381–389, http://dx.doi.org/10.1029/JZ070i002p00381.

Walsh J., The effect of cracks on the uniaxial elastic compression of rocks, *J. Geophys. Res.* **70**, 1965b, 399–411, http://dx.doi.org/10.1029/JZ070i002p00399.

White, D., Monitoring CO2 storage during EOR at the Weyburn-Midale Field, *Lead. Edge* **28** (7), 2009, 838-842, http://dx.doi.org/10.1190/1.3167786

White, J. C., Williams, G. A., Grude, S. and Chadwick, R. A., Utilizing spectral decomposition to determine the distribution of injected CO2 at the Snøhvit Field, *Geophys. Prospect.* **63** (5), 2015, 1213–1223. http://dx.doi.org/10.1111/1365-2478.12217

Wood A.B., A Textbook of Sound: Being an Account of the Physics of Vibrations with Special Reference to Recent Theoretical and Technical Developments, 1941, The Macmillan companyCompany.

Figures.

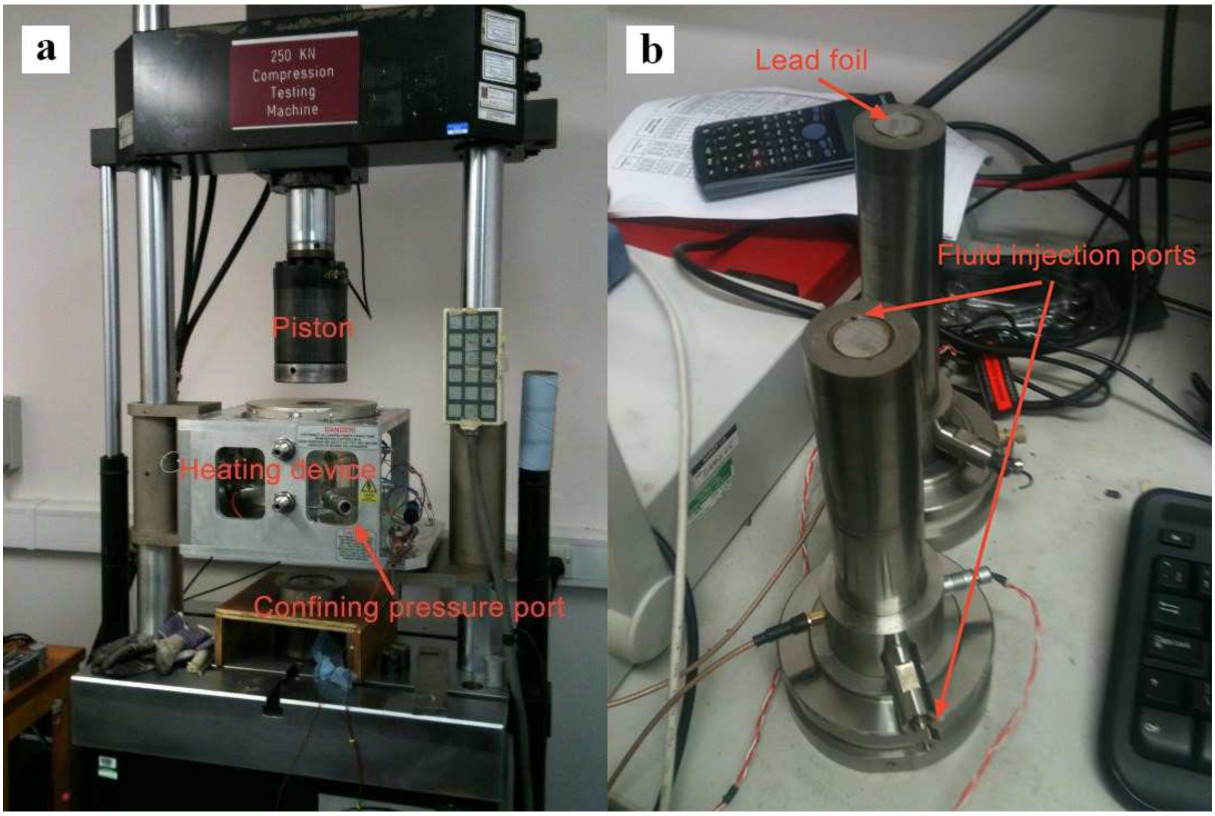

Figure 1. a) Triaxial cell equipped with sample heater used for sonic velocity determination. b) Steel platens placed on both sides of the core inside the heater used to generate sonic waves and to inject fluids.

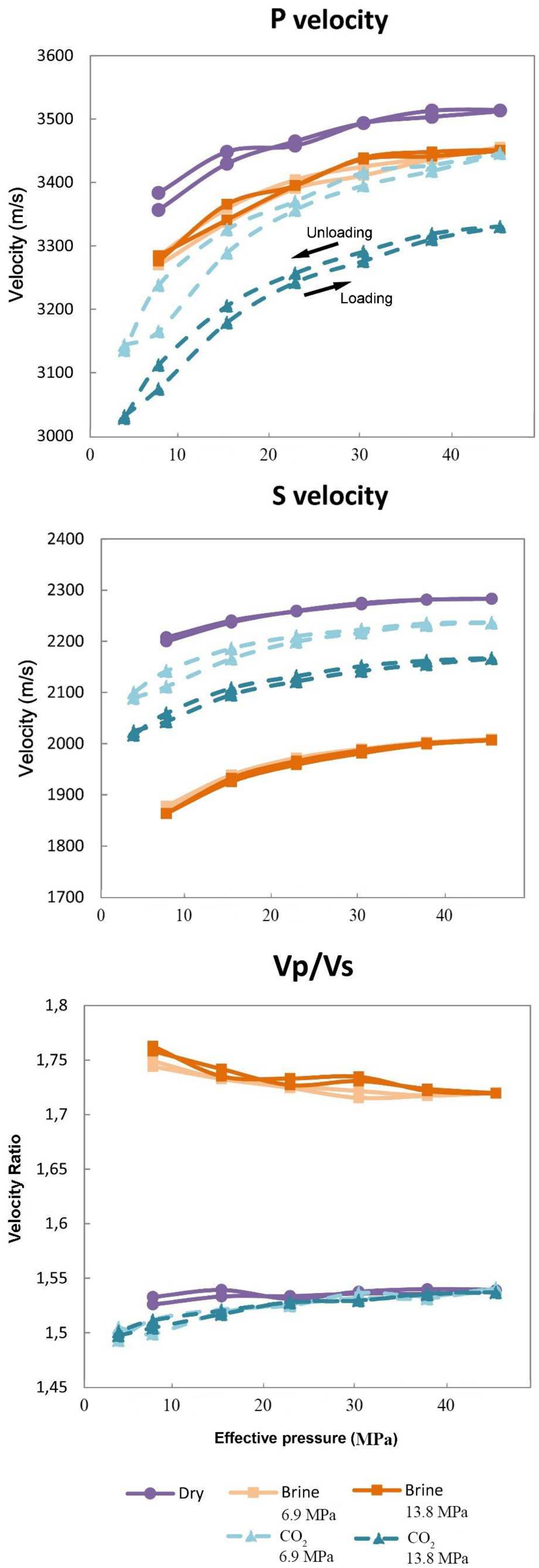
P velocity
Velocity (m/s)
Unloading
Loading
S velocity
Velocity (m/s)
Vp/Vs
Velocity Ratio
Effective pressure (MPa)
Dry
Brine 6.9 MPa
Brine 13.8 MPa
CO2 6.9 MPa
CO2 13.8 MPa

469

Figure 2. Effect of fluid composition and fluid pressure (either 6.9 or 13.8 MPa) on V_P, V_S and V_P/V_S ratio of core 3.1.

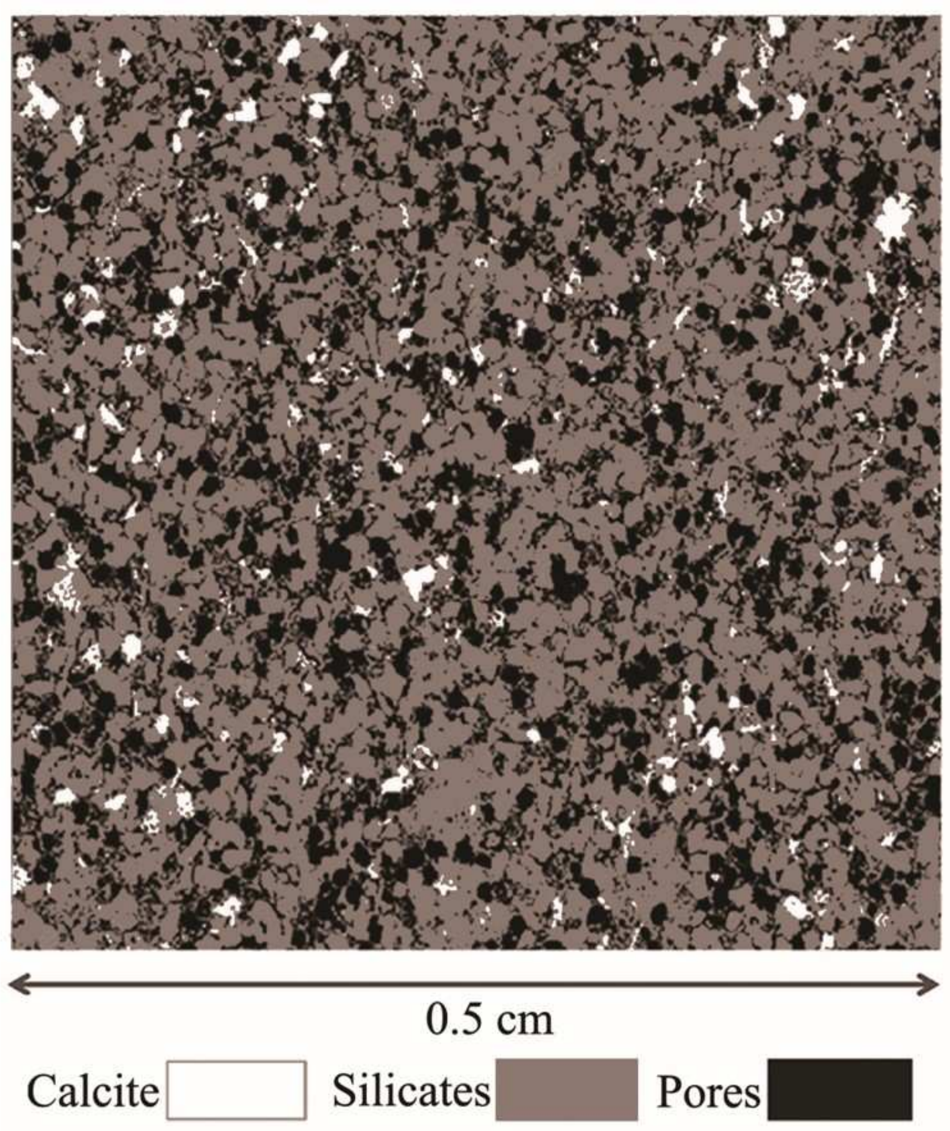

Figure 3. Thin section image showing calcite and pores distribution in Cayton Bay sandstone.

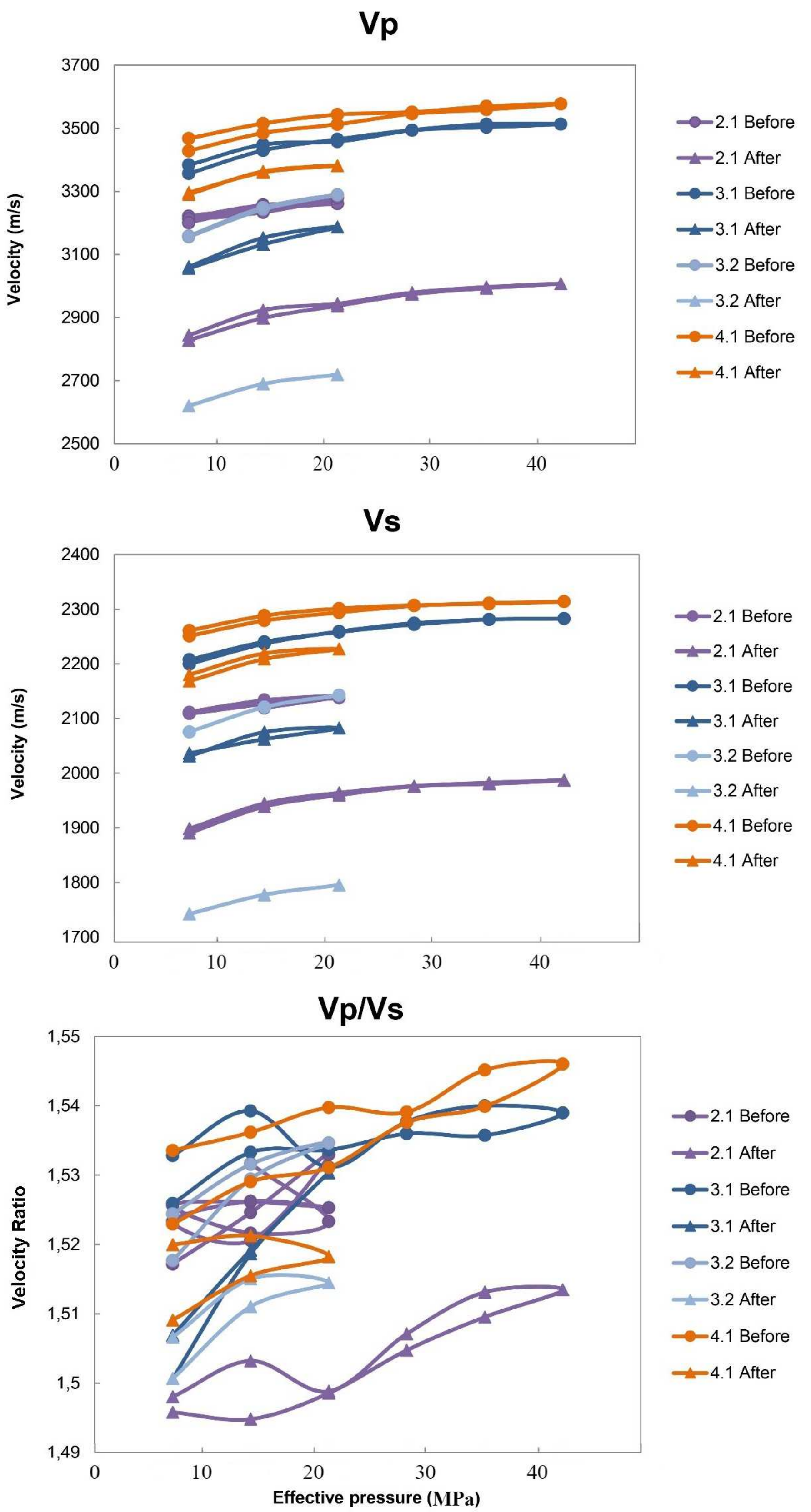

Figure 4. Comparison of V_P, V_S and V_P/V_S ratio before and after calcite dissolution for four cores.

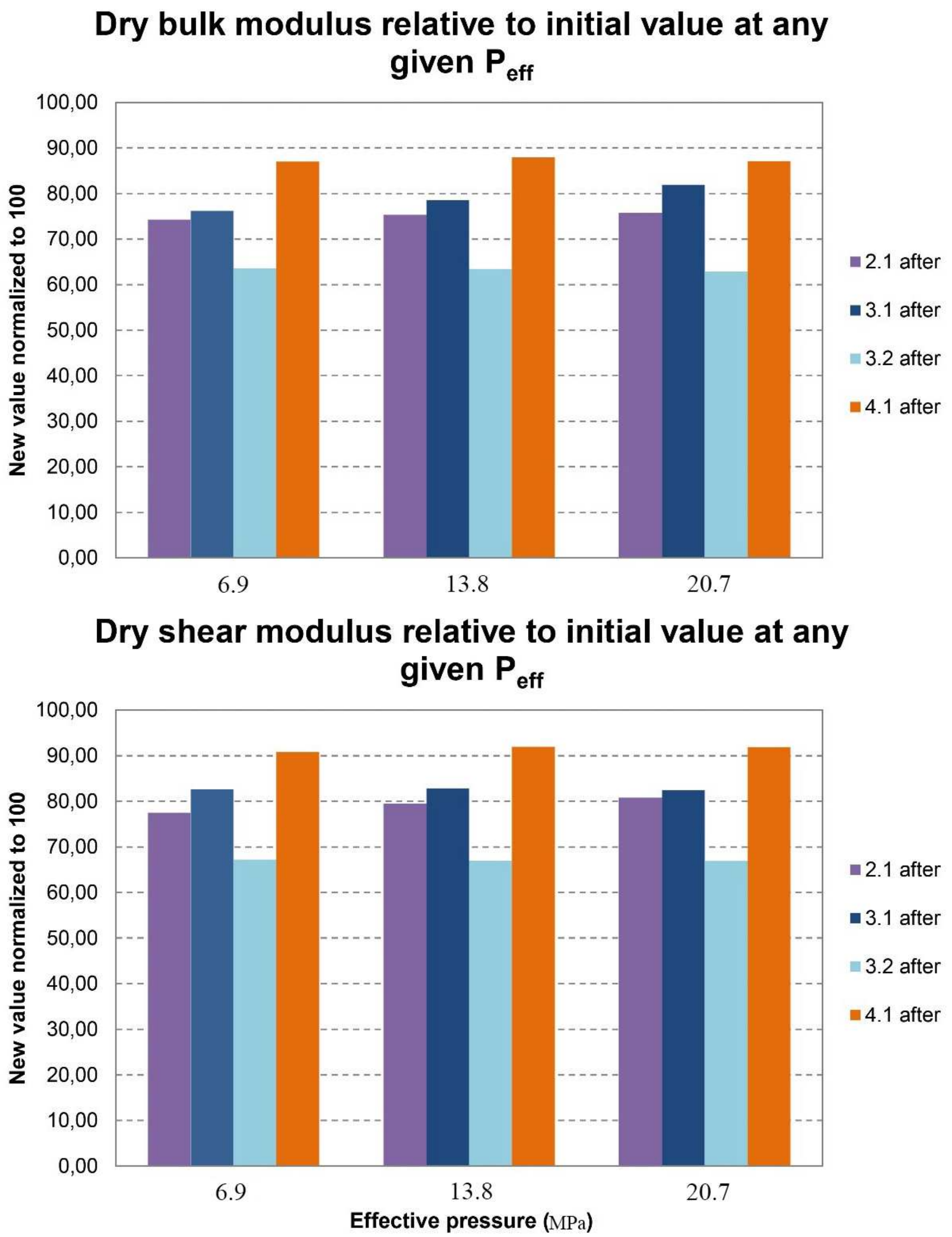

Figure 5. Change in bulk and shear moduli caused by calcite dissolution at constant effective pressure.

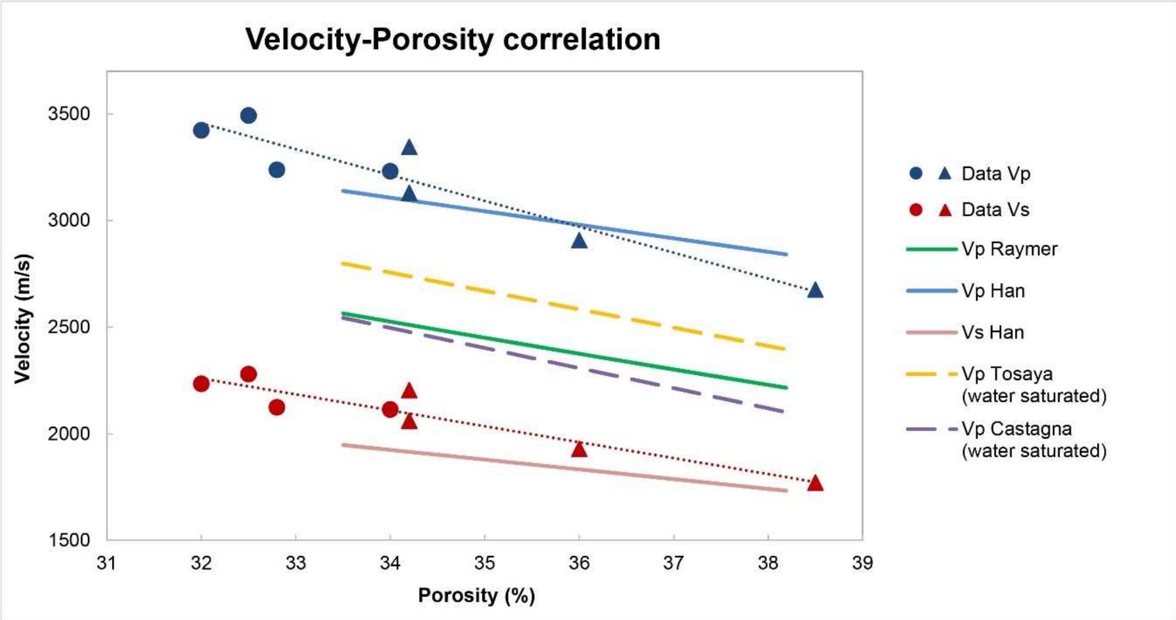

Figure 6. Comparison between empirical velocity-porosity correlations and experimental data. Unreacted core data is represented with circles and reacted core data is represented with triangles.

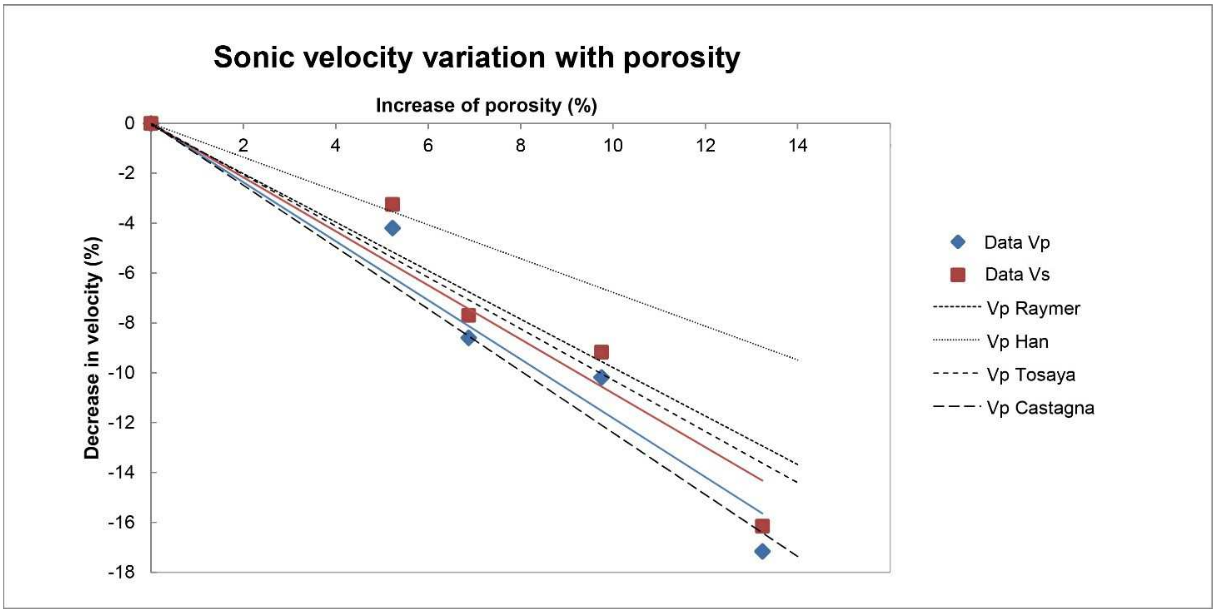

Figure 7. Comparison between empirical and experimental variation in velocity with porosity. Linear fit of the experimental data is also shown.

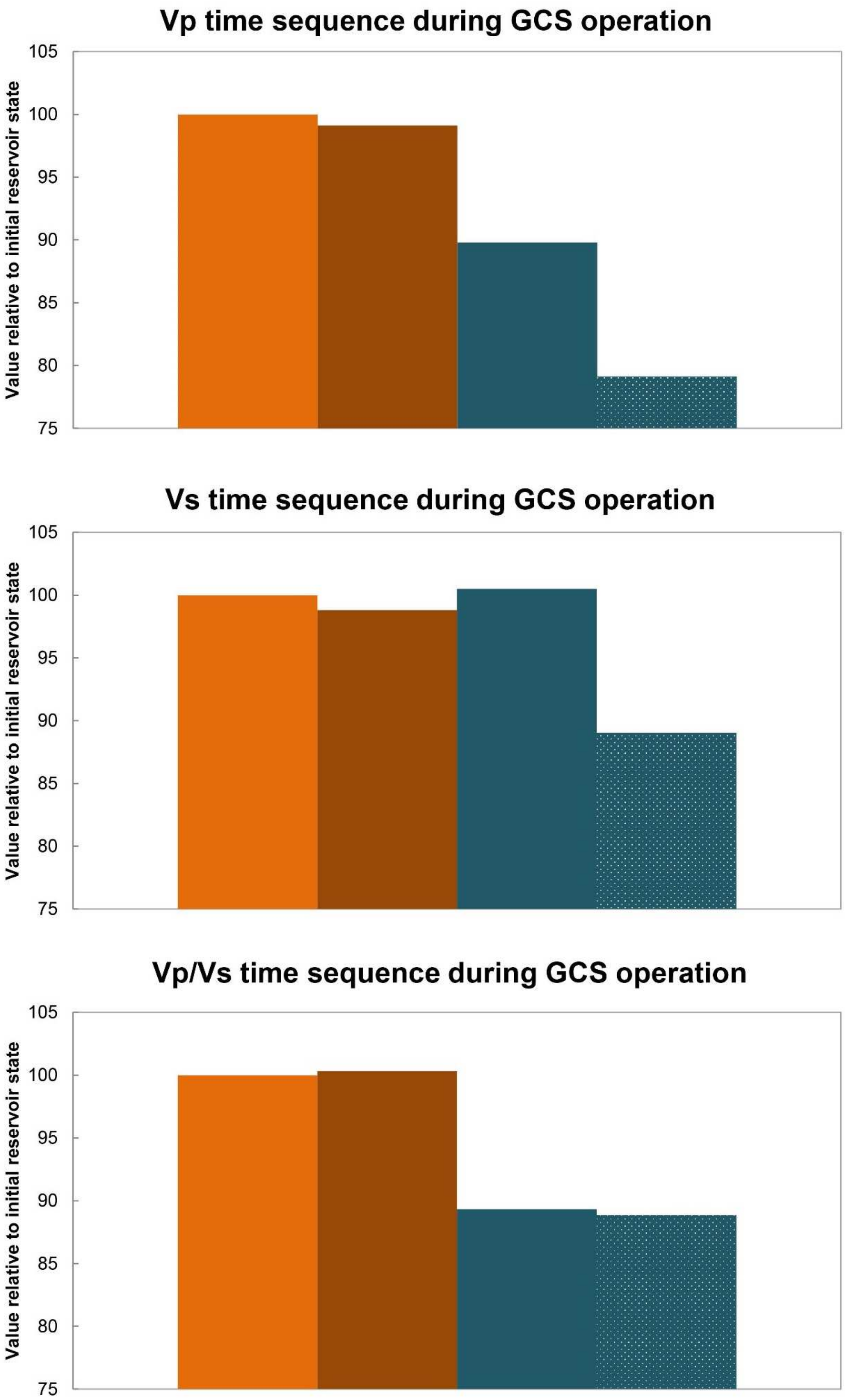

Figure 8. Normalized V_P, V_S and V_P/V_S evolution after brine pressurization, CO_2 invasion and CO_2 invasion plus calcite dissolution. Orange colour stands for brine saturated and blue for CO_2-saturated rock. Darker colours means higher fluid pressure. Calcite dissolution is represented as white dots

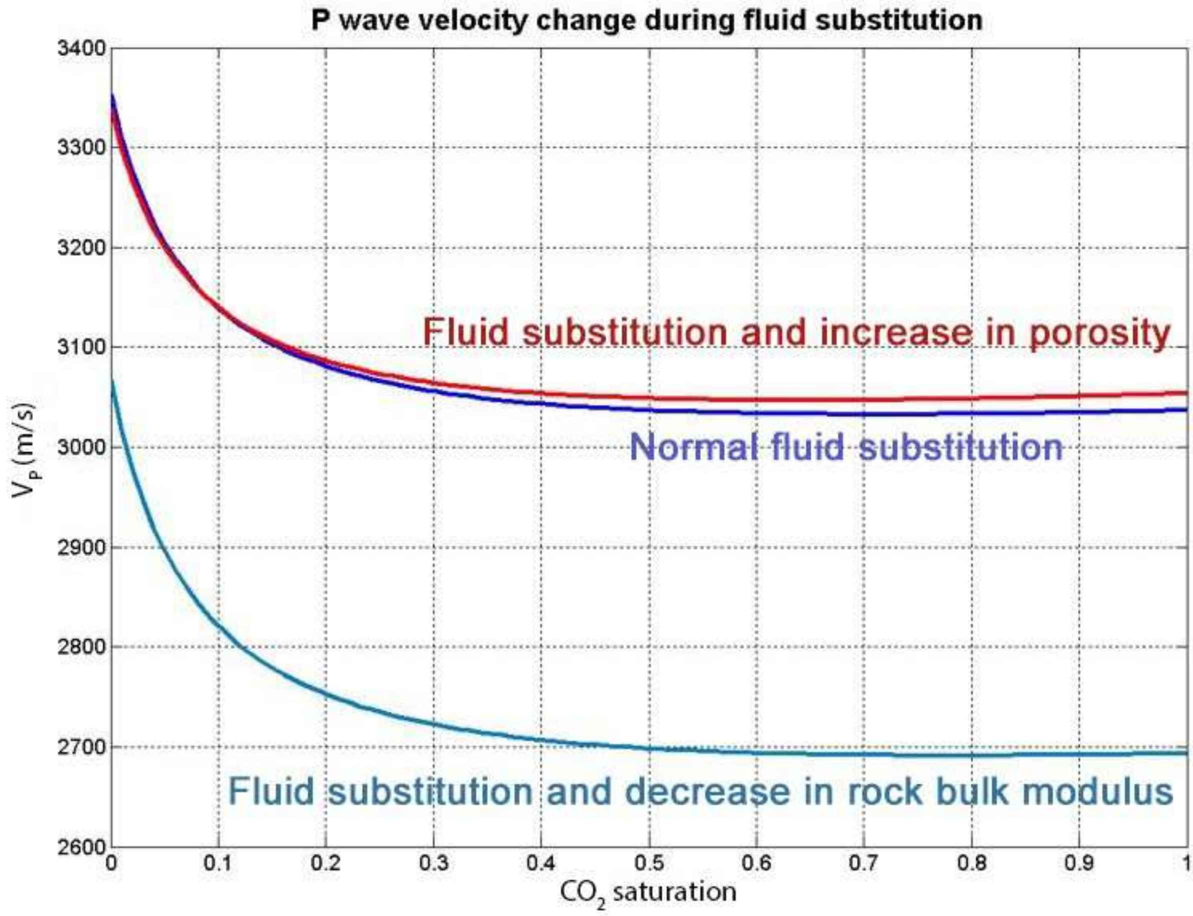

Figure 9. Fluid substitution effects on Vp according to Gassmann theory including the effect of a porosity change and the effect of a K_{dry} change.

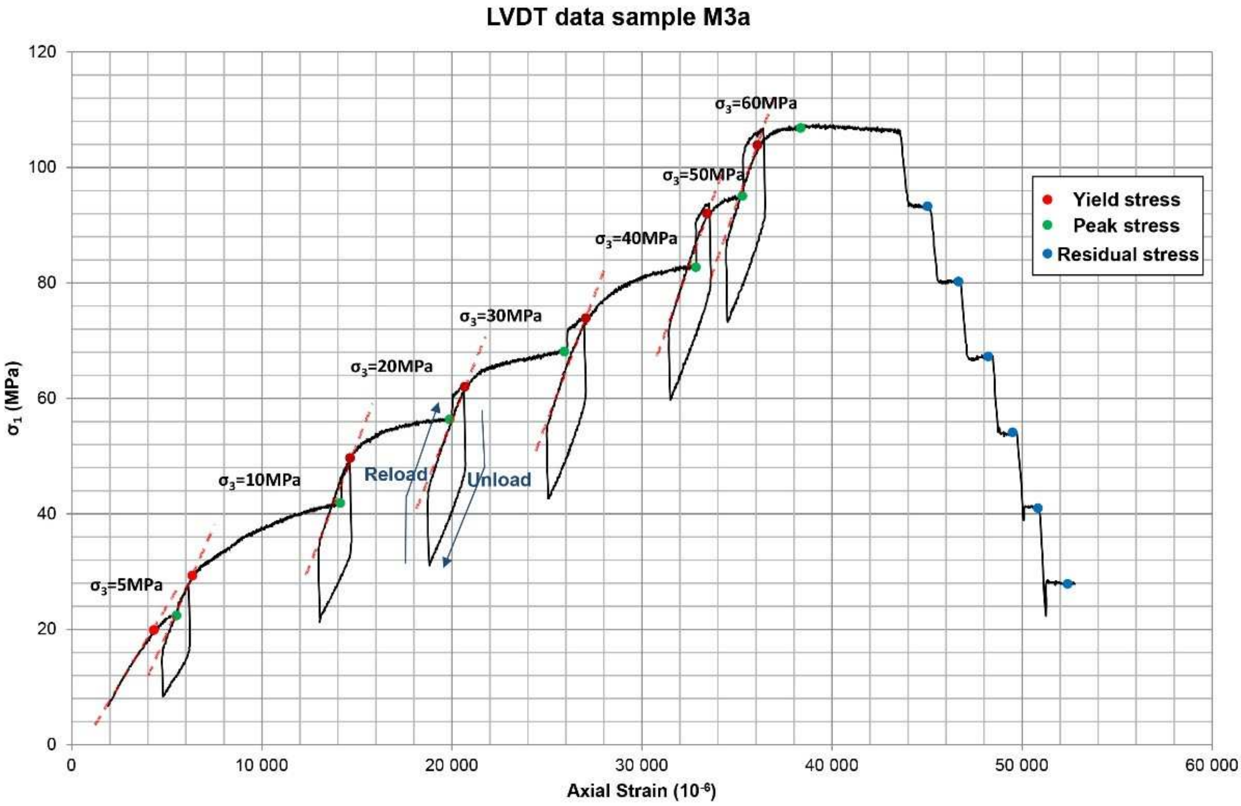

Figure 10. Example of multiple failure test data. The values of interest have been highlighted with dotted red guidelines to illustrate the yield stress determination. The unloading and reloading paths at the start of new confining pressure stage is also illustrated.

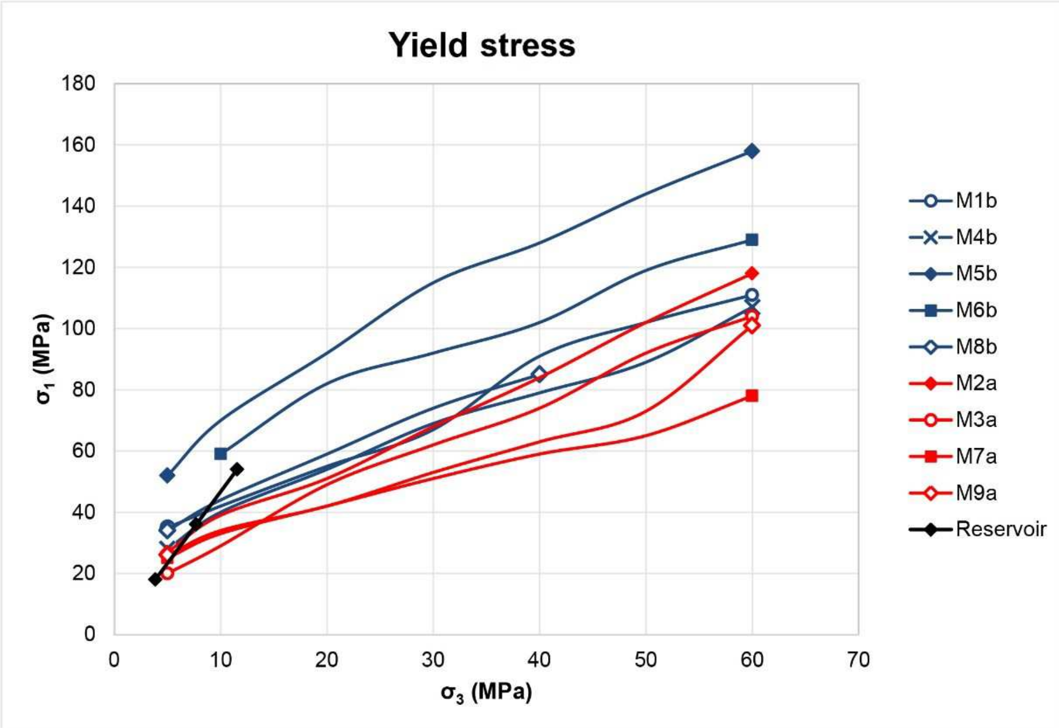

Figure 11. Yield stress envelopes for all cores and possible reservoir stress state at increasing depths of 1000, 2000 and 3000 m.

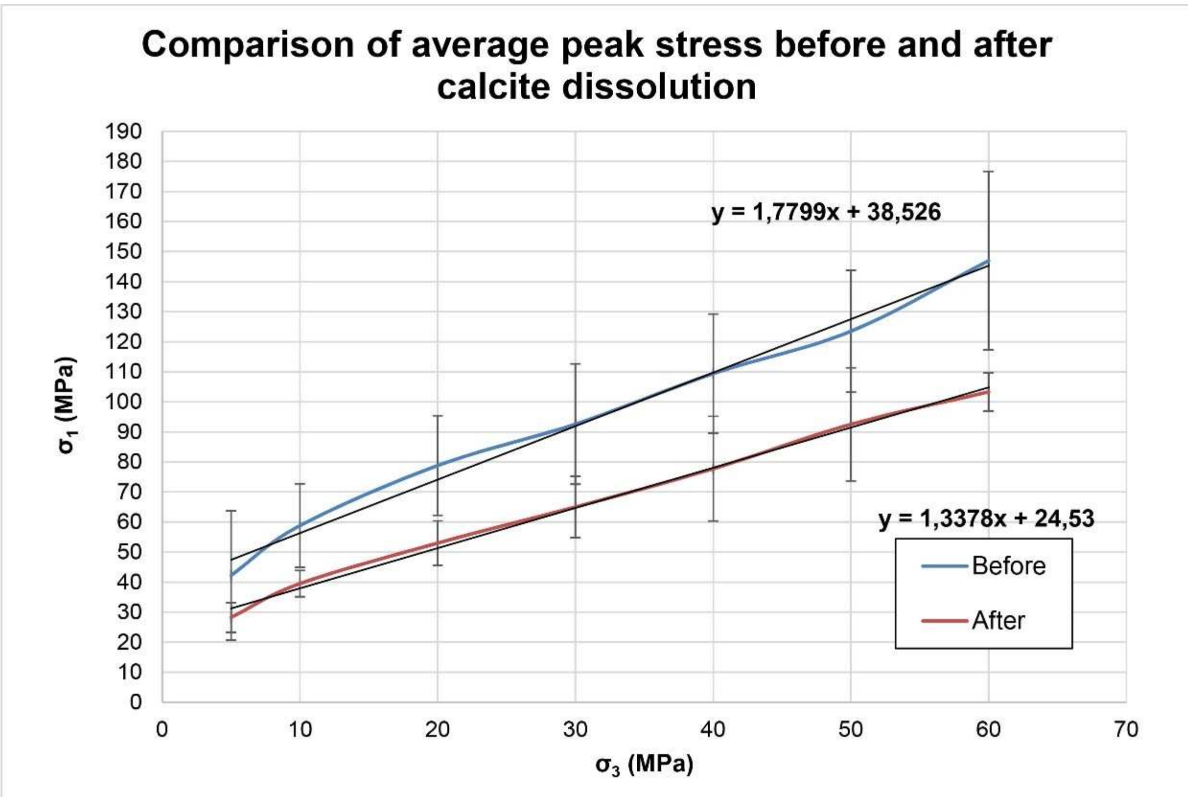

Figure 12. Linear fit of the average peak stress envelopes before and after dissolution (The bars represents two standard deviations from the mean). The effect of calcite dissolution on the rock cohesion (τ_0) is obvious (downward translation of the curve) while its effect on the angle of internal friction is more ambiguous (change in slope).

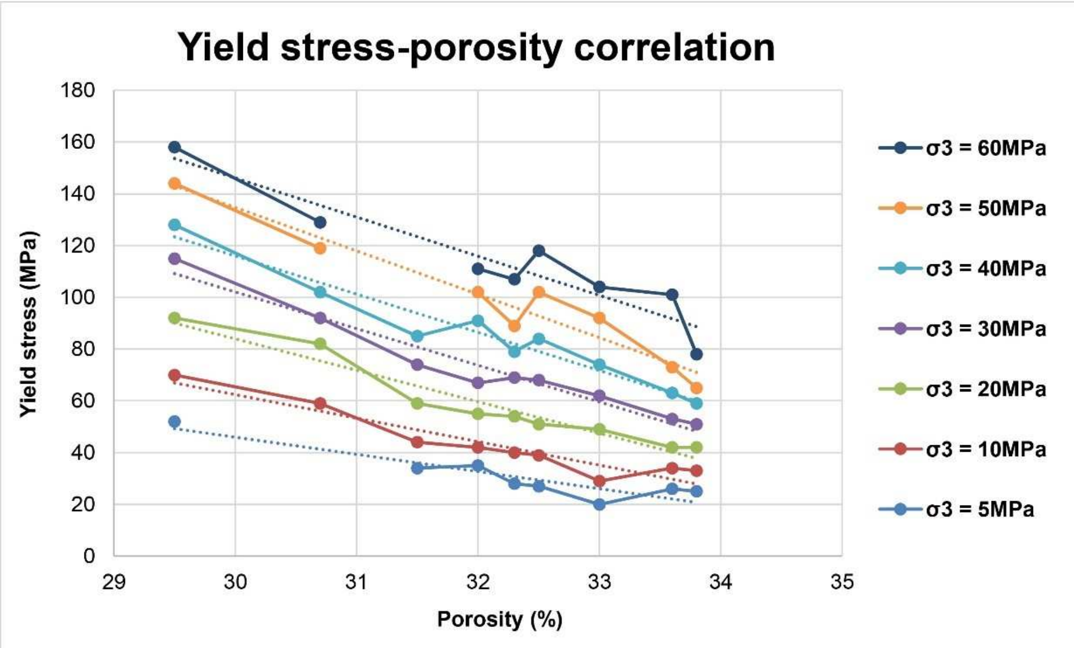

Figure 13. Experimental data showing the yield stress-porosity correlation. The results obtained on samples after calcite dissolution are represented as triangles and the results from unaltered samples are represented as discs. Every data points for a given porosity represent one single experiment. From left to right is presented the data from samples M5b, M6b, M8b, M1b, M4b, M2a, M3a, M9a and M7a (where “a” and “b” signifies “after” and “before” calcite dissolution).

Tables.

Table 1. Summary of sonic velocity experiments. All cores were drilled from the same sample block. Some cores were obtained by cutting a longer initial core in two (in that case they were

numbered N.1 and N.2). Some cores were used for multiple experiments at various fluid saturation and fluid pressure conditions.

Core number	Porosity before calcite dissolution	Porosity after calcite dissolution	Saturation conditions	Experiments before and after calcite dissolution	Pore pressure range (psi)
2.1	32.8	36	Dry at T=20°C and 50°C	yes	N/A
3.1	32.5	34.2	Dry/CO_2/Brine at T=50°C	yes	500-2000
3.2	34	38.5	Dry at T=50°C	yes	N/A
4.1	32.5	34.2	Dry/CO_2 at T=50°C	yes	2000-4000
4.2	35.5	N/A	Dry at T=20°C and 50°C	no	N/A

Table B1. Mineral bulk moduli and volume fraction used for the calculation of the K_m parameter.

Mineral Name	Volume fraction%	Bulk Modulus (GPa)
Quartz	76	37
Microcline	6	37
Mica	6	50
Calcite	5	77
Smectite	4	20
Kaolinite	1	1.5
Dolomite	1	95

Albite	1	76
Voigt Average		30
Reuss Average		39
VRH Average		34.5

Table B2. Fluid properties used for the Gassmann modelling

Fluid saturation	Pore pressure (psi)	Fluid density (kg/m^3)	System density	Fluid bulk modulus (GPa)
CO_2	1000	168	1835	0.009
CO_2	2000	666	1996	0.073
CO_2	3000	793	2038	0.176
Brine	1000	1026	2113	2.65
Brine	2000	1026	2113	2.69
Brine	3000	1026	2113	2.72